Supporting Information

Catalytic ignition of $N(CN)_2^-$ ionic liquid-H_2O_2 with zero-dimensional Cu-MOFs

Qing Cheng[ab], Yuan Yao[bc], Peihao Dou[b], Long Liu[c], Yingying Cao[*a], Yanqiang Zhang[*abc]

[a] College of Chemistry and Molecular Sciences, Henan University, Mingli Road North 379, 450046 Zhengzhou, China. E-mail: yqzhang@ipe.ac.cn.

[b] Zhengzhou Institute of Emerging Industrial Technology, East Third Ring Road and Jincheng Avenue Intersection East 300 meters, 450000, Zhengzhou, China.

[c] Institute of Process Engineering, Chinese Academy of Sciences, Beiertiao 1#, Zhongguancun, Haidian District, 100190 Beijing, China.

Content

Computational Details:

characterization of single X-ray diffraction

Data collections were performed using ϕ and ω scan. Non-hydrogen atoms located from the difference Fourier maps were refined anisotropically by full-matrix least-squares on F^2, using SHELXS-97. All hydrogen atoms were included in the calculated positions and refined isotropically using a riding model. Determinations of the crystal system, orientation matrix, and cell dimensions were performed according to the established procedures. Lorentz polarization and multiscan absorption correction were applied. All calculations were performed using SHELXL 97 and PLATON 99. The crystallographic data for **1-5** are listed in Table 1. Moreover, the selected bonds distances and bond angles are summarized in Supporting Information Table S1.

DFT calculations

Density function theory (DFT) calculations were carried out using Gaussian 16 programs[1] throughout this manuscript. Geometric optimizations of the reactants, transition states, and products were performed using TPSSh hybrid function[2]. The standard 6-31G(d,p) basis set[3-5] for H, C, N and O was used. For the Cu atoms, the SDD basis set and its corresponding effective core potential[6] was used. Harmonic vibration frequency calculations were performed for all stationary points to confirm them as a local minima or transition state. The intrinsic reaction coordinate (IRC) scheme[7-8] was applied for the calculations of the reaction coordinates to confirm whether or not the transition states were directly connected to the reactants and products. Gibbs free energy (G) was calculated using Shermo software[9].

Heats of Formation

The heat of formation (ΔH_f) of MOFs were calculated using the following reaction[10]:

$$\mathrm{Cu(s)} + \mathrm{C(s)} + H_2(g) + \mathrm{O_2}(g) + \mathrm{N_2}(g) \rightarrow C_aH_bCu_cO_dN_e$$

These calculations were performed by using CP2K 2023.1[11]. Hybrid function PBE0 function[12] combined with Grimme D3 dispersion correction[13] were employed. And the plane wave energy cutoff was set as 400 eV. All structure was first optimized under the DZVP-MOLOPT-SR-GTH basis set[14], and then the single point energy was calculated under the pob-TZVP basis set[15]. The optimization was considered to converge when the following criteria were met: a maximum energy change of 10^{-6} eV per atom and a maximum force on atom of 0.00045 eV·Å^{-1}. The input files were obtained with the assistance of the Multiwfn software[16].

The calculation results of the catalysts are shown in Table S1.

Table S1 Heats of formation of MOFs **1**-**4**.

Sample	MOF 1	MOF 2	MOF 3	MOF 4
ΔH_f (solid, 298K, kJ·mol^{-1})	-3642.4	-3575.1	-8454.3	-9802.4

To the MOF + $[BMIM]N(CN)_2$ mixtures, the heat of formations were calculated through Equations 1-4. MOF: Fuel = x: y = 0.99:0.01, 0.97:0.03, 0.95:0.05, 0.93:0.07, 0.91:0.09, 0.89:0.11, 0.87:0.13, 0.85:0.15. The ΔH_f of $[BMIM]N(CN)_2$ was obtained from the literature[17].

$$n_{MOF} = \frac{x}{M_{MOF}} \tag{1}$$

$$n_{IL} = \frac{y}{M_{IL}} \tag{2}$$

$$n_{sum} = n_{MOF} + n_{IL} = \frac{x}{M_{MOF}} + \frac{y}{M_{IL}} \tag{3}$$

$$\Delta_f H_{mix} = \frac{n_{MOF}}{n_{sum}} * \Delta_f H_{MOF} + \frac{n_{IL}}{n_{sum}} * \Delta_f H_{IL} \tag{4}$$

References

1 Gaussian 16, Revision C.01, M. Frisch, G. Trucks, H. Schlegel, G. Scuseria, M. Robb, J. Cheeseman, G. Scalmani, V. Barone, G. Petersson, H. Nakatsuji, X. Li, M. Caricato, A. Marenich, J. Bloino, B. Janesko, R. Gomperts, B. Mennucci, H. Hratchian, J. Ortiz, A. Izmaylov, J. Sonnenberg, Y. Williams, F. Ding, F. Lipparini, F. Egidi, J. Goings, B. Peng, A.Petrone, T. Henderson, D. Ranasinghe, V. Zakrzewski, J. Gao, N. Rega, G. Zheng, W.Liang, M. Hada, M. Ehara, K. Toyota, R. Fukuda, J. Hasegawa, M. Ishida, T. Nakajima, Y. Honda, O. Kitao, H. Nakai, T. Vreven, K. Throssell, J. Montgomery, J. Peralta, F. Ogliaro, M. Bearpark, J. Heyd, E. Brothers, K. Kudin, V. Staroverov, T. Keith, R.Kobayashi, J. Normand, K. Raghavachari, A. Rendell, J. Burant, S. Iyengar, J. Tomasi, M.Cossi, J. Millam, M. Klene, C. Adamo, R. Cammi, J. Ochterski, R. Martin, K.Morokuma, O. Farkas, J. Foresman, D. Fox, Inc. Gaussian,, Wallingford CT, 2016.

2 V. Staroverov, G. Scuseria, J. Tao, and J. Perdew, *J. Chem. Phys.*, 2003, **119**, 12129-12137.

3 W. Hehre, R. Ditchfield and J. Pople, *J. Chem. Phys.*, 1972, **56**, 5255-5257.

4 M. Francl, W. Pietro, W. Hehre, J. Binkley, M. Gordon, D. DeFrees and J. Pople, *J. Chem. Phys.*, 1982, **77**, 3654-3665.

5 T. Clark, J. Chandrasekhar and P. Schleyer, *J. Comp. Chem.*, 1983, **4**, 294-301.

6 M. Dolg, U. Wedig, H. Stoll, and H. Preuss, *J. Chem. Phys.*, 1987, **86**, 866-872.

7 K. Fukui, *J. Phys. Chem.*, 1970, **74**, 4161-4163.

8 K. Fukui, *Acc. Chem. Res.*, 1981, **14**, 363-368.

9 T. Lu, Q. Chen, *Comput. Theor. Chem.*, 2021, **1200**, 113249.

10 O. Jobin, C. Mottillo, H. Titi, *Chem. Sci.*, 2022, **13**, 3424-3436.

11 T. Kühne, M. Iannuzzi, B. Del,. *J. Chem. Phys.*, 2020, **152**. 194103.
12 C Adamo, V Barone. *J. Chem. Phys.*, 1999, **110**, 6158-6170.
13 S. Grimme, J. Antony, S. Ehrlich, *J. Chem. Phys.*, 2010, **132**. 154104.
14 V. Vondele, J. Hutter, *J. Chem. Phys.*, 2007, **127**. 114105.
15 M. Peintinger, D. Oliveira, T. Bredow, *J. Comput. Chem.*, 2013, **34**, 451-459.
16 T. Lu, F. Chen, *J. Comput. Chem.,* 2012, **33**, 580-592.
17 A. Thomas, K. Stober, R. Otaibi, *52nd AIAA/SAE/ASEE Joint Propulsion Conference*, 2016.

Table S2 Crystallographic data and structure refinement details for MOFs **1**-**4**

MOF	**1**	**2**	**3**	**4**
formula	$C_8H_{12}Cu_2N_{22}O_{2.5}$	$C_8H_{12}Cu_2N_{22}O_{2.4}$	$C_{14}H_{20}Cu_2$	$C_{18}H_{28}Cu_2O_{10}$
fw	583.48	581.88	475.40	531.5
T/K	118.1	123.0	273	273
crystal system	orthorhombic	orthorhombic	monoclinic	monoclinic
space group	P2na	Pbcn	P 2_1/n	C 2/c
a (Å)	13.4957(5)	15.0819(19)	7.6004(4)	37.398(3)
b (Å)	9.9441(6)	13.4307(14)	9.0452(5)	6.9621(4)
c (Å)	15.0536(7)	9.9113(14)	14.0935(9)	18.7788(14)
α (deg)	90	90	90	90
β (deg)	90	90	97.329(2)	97.255(3)
γ (deg)	90	90	90	90
V (Å^3)	2020.24(16)	2007.6(4)	960.97(10)	4850.3(6)
Z	4	4	2	8
ρ (g·cm^{-3})	1.918	1.925	1.643	1.456
abs coeff (mm^{-1})	2.172	2.185	2.260	1.799
F (000)	1168	1165	484.0	2192.0
GOF	1.043	1.014	0.943	1.089
data/restraints/parame	3441/19/326	1949/6/159	3809/0/139	5579/376/277
$R_1(I > 2\sigma(I))^a$	0.0438	0.0934	0.0292	0.0529
$wR_2(I > 2\sigma(I))^b$	0.0963	0.2067	0.0789	0.1439

$^aR_1 = \sum||F_0| - |F_c||/\sum|F_0|$. $^bwR_2 = \{\sum[w(F_0^2 - F_c^2)^2]/\sum[w(F_0^2)^2]\}^{1/2}$.

Table S3 Selected bond lengths and bond angles of MOF **1**

Atom	Length (Å)	Atom	Length (Å)
Cu1-N18	2.013(7)	Cu2-N16^{2}	2.434(6)
Cu1-N22	1.997(8)	Cu2-N10	1.998(7)
Cu1-N4^{1}	2.292(7)	Cu2-N19	2.011(7)
Cu1-N14	2.031(7)	Cu2-N20	2.006(7)
Cu1-N21	2.031(8)	N4-Cu1^{1}	2.292(7)
Cu2-N6	2.013(8)	N16-Cu2^{2}	2.434(6)
Atom	**Angle (°)**	**Atom**	**Angle (°)**
N18-Cu1-N4^{1}	96.8(3)	N19-Cu2-N16^{2}	83.2(3)
N18-Cu1-N14	85.5(3)	N20-Cu2-N6	173.9(3)
N18-Cu1-N21	169.1(3)	N20-Cu2-N16^{2}	89.8(3)
N22-Cu1-N18	91.7(3)	N20-Cu2-N19	92.0(3)
N22-Cu1-N4^{1}	92.5(3)	N5-N6-Cu2	122.3(5)
N22-Cu1-N14	171.1(3)	C1-N6-Cu2	132.0(5)
N22-Cu1-N21	92.8(3)	N17-N18-Cu1	121.5(5)
N14-Cu1-N4^{1}	96.2(3)	C7-N18-Cu1	131.7(5)
N14-Cu1-N21	88.5(3)	N3-N4-Cu1^{1}	124.1(5)
N21-Cu1-N4^{1}	93.0(3)	N5-N4-Cu1^{1}	125.3(5)
N6-Cu2-N16^{2}	94.5(3)	N15-N16-Cu2^{2}	127.8(6)
N10-Cu2-N6	85.7(3)	N17-N16-Cu2^{2}	121.9(4)
N10-Cu2-N16^{2}	93.9(3)	C5-N14-Cu1	133.7(7)
N10-Cu2-N19	176.6(3)	N9-N10-Cu2	121.0(5)
N10-Cu2-N20	89.8(3)	C4-N10-Cu2	134.9(7)
N19-Cu2-N6	92.6(3)		

Noted: ^{1}+X,-1-Y,-1-Z; ^{2}+X,-2-Y,-1-Z

Table S4 Selected bond lengths and bond angles of MOF **2**

Atom	Length (Å)	Atom	Length (Å)
Cu1-N9^{1}	2.013(8)	Cu1-N1^{1}	1.987(9)
Cu1-N7^{2}	2.329(7)	N9-Cu1^{1}	2.013(8)
Cu1-N2	2.004(8)	N7-Cu1^{2}	2.329(7)
Cu1-N10	2.008(7)		
Atom	**Angle (°)**	**Atom**	**Angle (°)**
N9^{1}-Cu1-N7^{2}	96.5(3)	N11-Cu1-N2	174.5(4)
N2-Cu1-N9^{1}	84.7(3)	N11-Cu1-N10	92.4(4)
N2-Cu1-N7^{2}	96.1(3)	N8-N9-Cu1^{1}	122.3(6)
N2-Cu1-N10	90.0(3)	C4-N9-Cu1^{1}	131.8(6)
N10-Cu1-N9^{1}	170.4(3)	N8-N7-Cu1^{2}	122.7(6)
N10-Cu1-N7^{2}	92.0(3)	N6-N7-Cu1^{2}	126.2(6)
N11-Cu1-N9^{1}	92.2(3)	C1-N2-Cu1	133.5(7)
N11-Cu1-N7^{2}	88.8(4)	N3-N2-Cu1	120.8(6)

Noted: ^{1}-X,2-Y,-Z; ^{2}-X,+Y,-1/2-Z

Table S5 Selected bond lengths and bond angles of MOF **3**

Atom	Length (Å)	Atom	Length (Å)
Cu1-Cu1[1]	2.6201(3)	Cu1-O4	1.9678(11)
Cu1-O1[1]	1.9561(11)	Cu1-O5	2.1812(12)
Cu1-O2	1.9473(11)	O1-Cu1[1]	1.9561(11)
Cu1-O3[1]	1.9831(11)	O3-Cu1[1]	1.9831(11)
Atom	**Angle (°)**	**Atom**	**Angle (°)**
O1[1]-Cu1-Cu1[1]	81.81(4)	O3[1]-Cu1-O5	91.87(5)
O1[1]-Cu1-O3[1]	89.60(5)	O4-Cu1-Cu1[1]	85.68(3)
O1[1]-Cu1-O4	90.17(5)	O4-Cu1-O3[1]	168.77(5)
O1[1]-Cu1-O5	93.20(5)	O4-Cu1-O5	99.35(5)
O2-Cu1-Cu1[1]	86.94(4)	O5-Cu1-Cu1[1]	172.96(5)
O2-Cu1-O1[1]	168.75(5)	C3-O1-Cu1[1]	125.33(11)
O2-Cu1-O3[1]	89.38(5)	C3-O2-Cu1[1]	120.14(10)
O2-Cu1-O4	88.66(5)	C6-O3-Cu1[1]	123.90(9)
O2-Cu1-O5	98.03(5)	C6-O4-Cu1[1]	122.18(10)
O3[1]-Cu1-Cu1[1]	83.17(3)	C7-O5-Cu1[1]	124.68(12)

Noted: [1]1-X,1-Y,1-Z

Table S6 Selected bond lengths and bond angles of MOF **4**

Atom	Length (Å)	Atom	Length (Å)
Cu1-Cu1[1]	2.5835(8)	Cu2-Cu2[2]	2.5823(8)
Cu1-O1	1.944(3)	Cu2-O6	1.953(3)
Cu1-O2[1]	1.955(3)	Cu2-O7[2]	1.962(3)
Cu1-O3	1.957(3)	Cu2-O8	1.959(3)
Cu1-O4[1]	1.947(3)	Cu2-O9[2]	1.952(3)
Cu1-O5	2.135(3)	Cu2-O10	2.136(3)
O2-Cu1[1]	1.955(3)	O7-Cu2[2]	1.962(3)
O4-Cu1[1]	1.947(3)	O9-Cu2[2]	1.952(3)
Atom	**Angle (°)**	**Atom**	**Angle (°)**
O1-Cu1-Cu1[1]	84.65(9)	O6-Cu2-Cu2[2]	84.41(9)
O1-Cu1-O2[1]	168.78(13)	O6-Cu2-O7[2]	168.64(12)
O1-Cu1-O3	88.80(15)	O6-Cu2-O8	89.84(15)
O1-Cu1-O4[1]	90.96(13)	O6-Cu2-O10	95.95(12)
O1-Cu1-O5	96.23(13)	O7[2]-Cu2-Cu2[2]	84.34(9)
O2[1]-Cu1-Cu1[1]	84.28(10)	O7[2]-Cu2-O10	95.35(12)
O2[1]-Cu1-O3	88.30(17)	O8-Cu2-Cu2[2]	85.35(10)
O2[1]-Cu1-O5	94.85(13)	O8-Cu2-O7[2]	87.69(16)
O3-Cu1-Cu1[1]	84.55(9)	O8-Cu2-O10	96.70(13)
O3-Cu1-O5	95.81(13)	O9[2]-Cu2-Cu2[2]	83.61(9)
O4[1]-Cu1-Cu1[1]	83.95(8)	O9[2]-Cu2-O6	89.86(14)
O4[1]-Cu1-O2[1]	89.72(15)	O9[2]-Cu2-O7[2]	90.45(15)
O4[1]-Cu1-O3	168.47(12)	O9[2]-Cu2-O8	168.93(13)

O4[1]-Cu1-O5	95.67(12)	O9[2]-Cu2-O10	94.33(13)
O5-Cu1-Cu1[1]	179.05(11)	O10-Cu2-Cu2[2]	177.91(10)
C4-O1-Cu1	123.3(3)	C13-O6-Cu2	123.6(3)
C4-O2-Cu1[1]	122.8(3)	C13-O7-Cu2[2]	123.3(3)
C8-O3-Cu1	123.1(3)	C17-O8-Cu2	122.3(3)
C8-O4-Cu1[1]	124.3(2)	C17-O9-Cu2[2]	124.8(3)
C9-O5-Cu1	127.2(3)	C18-O10-Cu2	125.4(3)

Noted: [1]2-X,1-Y,1-Z; [2]3/2-X,3/2-Y,1-Z

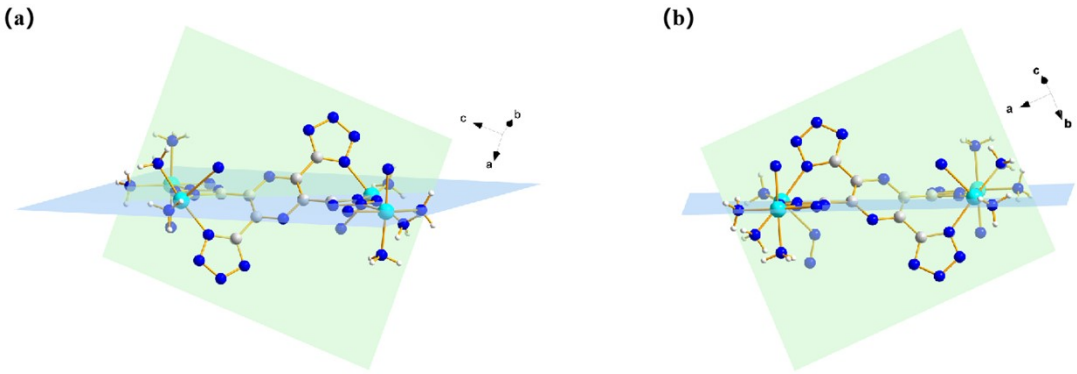

Fig. S1 Angles of the plane formed by the para-tetrazole ring in **1** (a), and **2** (b)

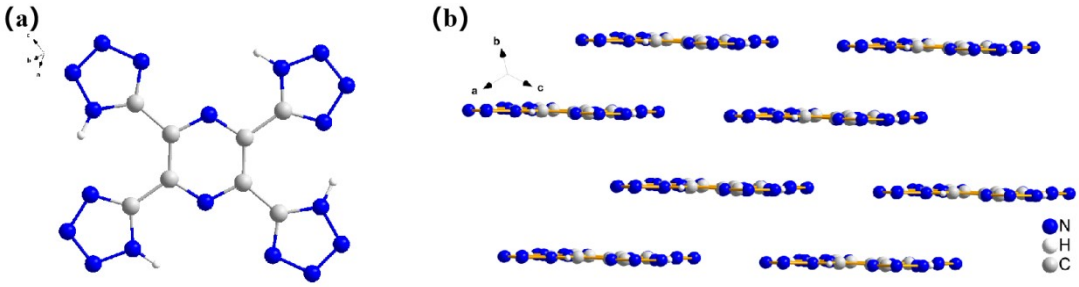

Fig. S2 Structures of H_4TTP single molecule (a) and stacking diagram (b)

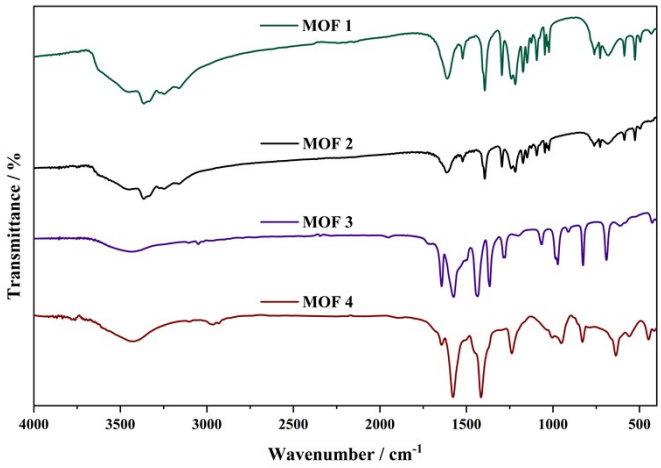

Fig. S3 FT-IR spectra of MOFs **1-4**

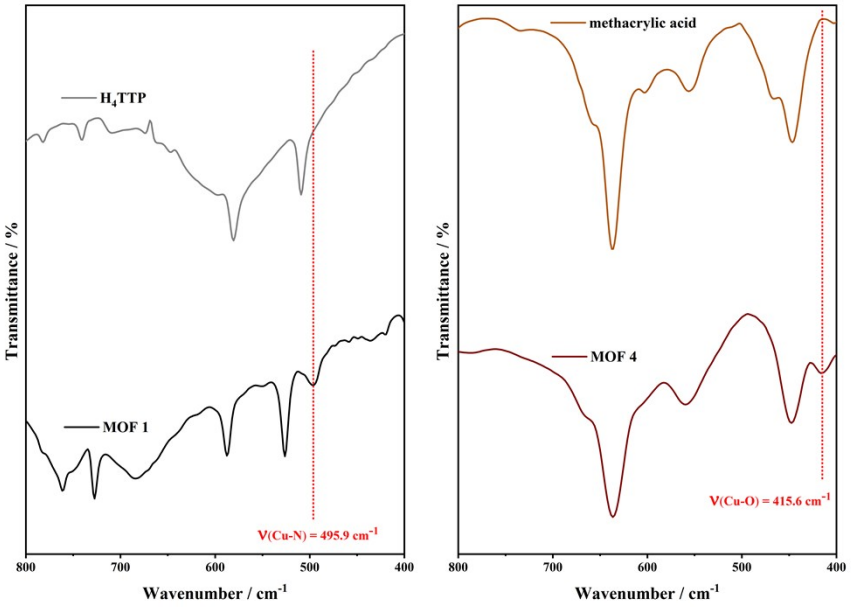

Fig. S4 FT-IR spectra of H_4TTP, methacrylic acid and MOFs **1/4**

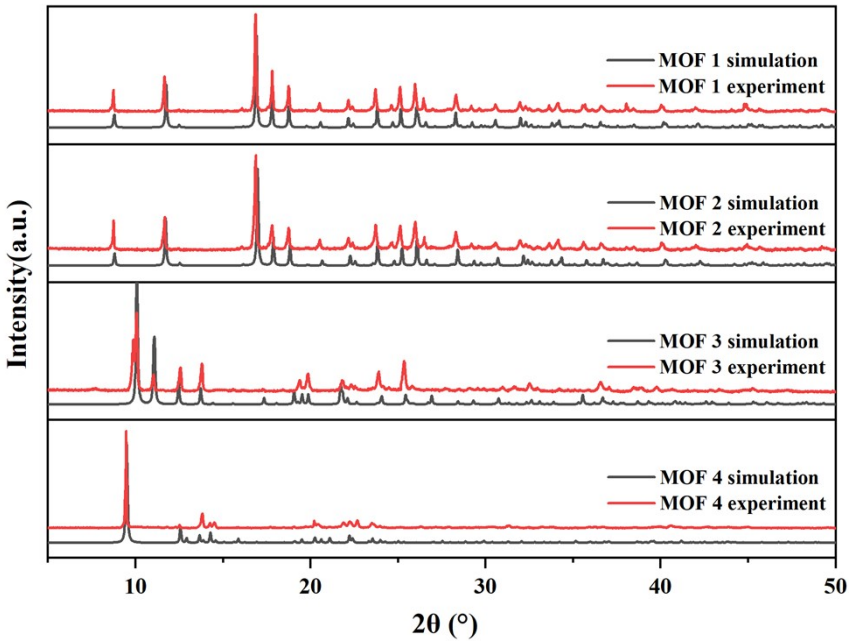

Fig. S5 PXRD patterns for MOFs **1-4**.

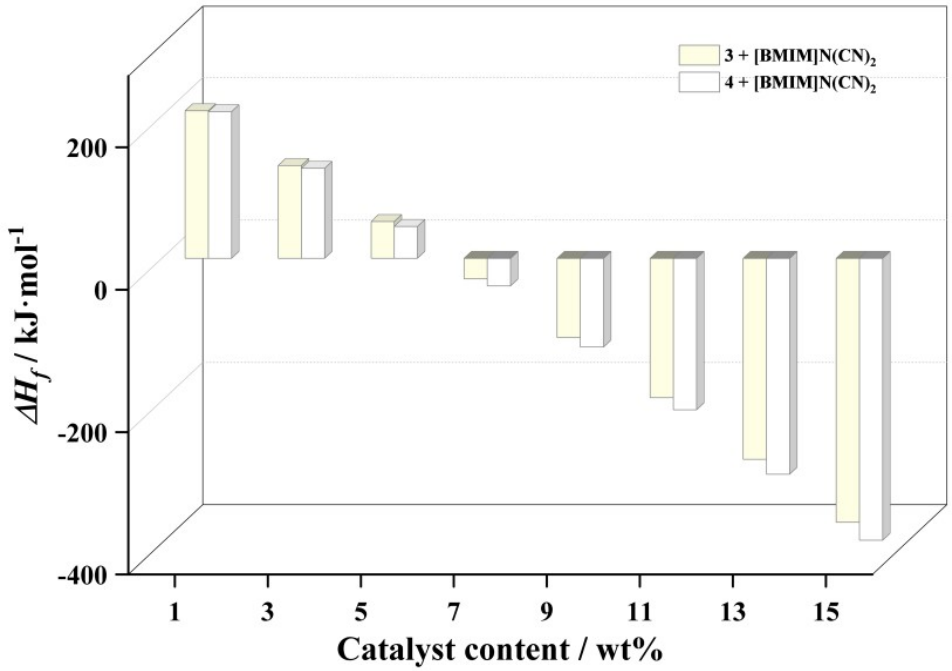

Fig. S6 ΔH_f of MOFs **3/4** + $[BMIM]N(CN)_2$

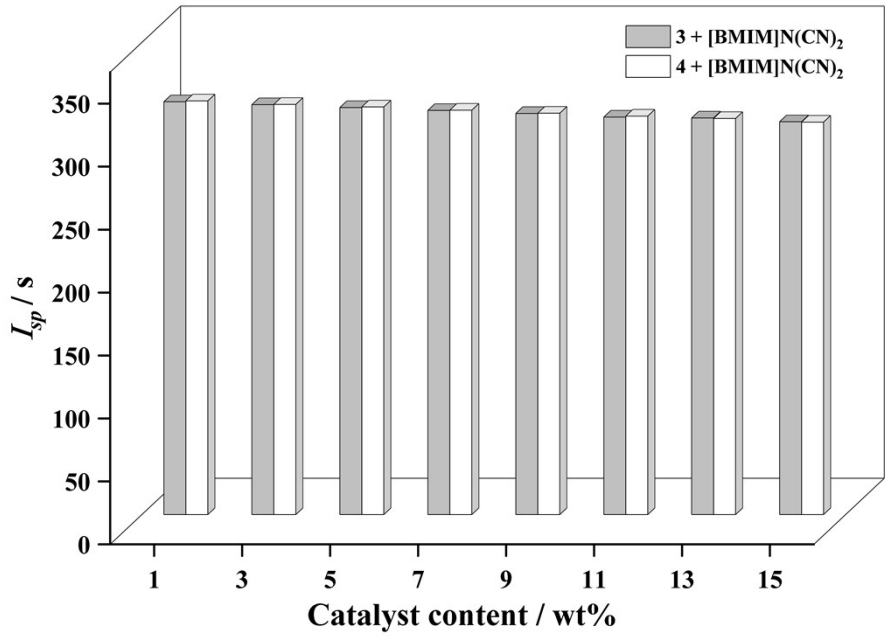

Fig. S7 I_{sp} of MOFs **3/4** + $[BMIM]N(CN)_2$

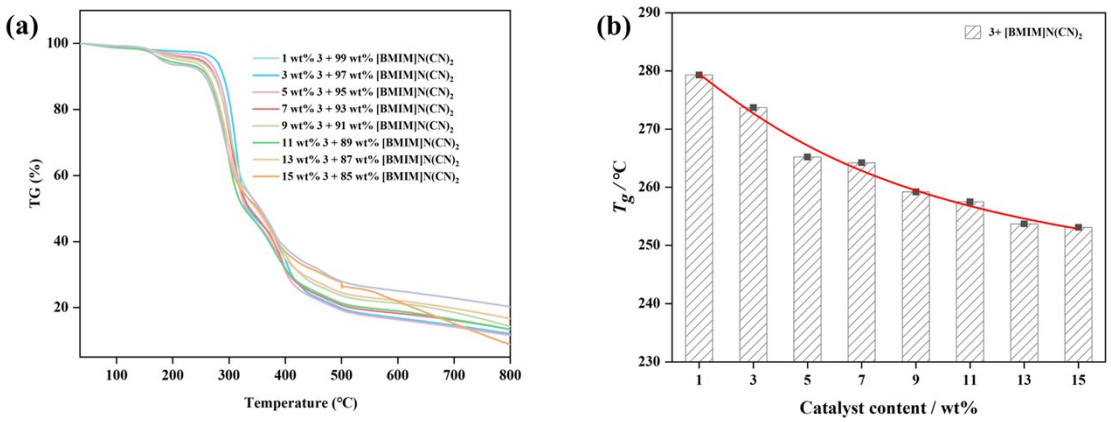

Fig. S8 Decomposition temperatures (a) and variation rule (b) of MOF **3** + $[BMIM]N(CN)_2$

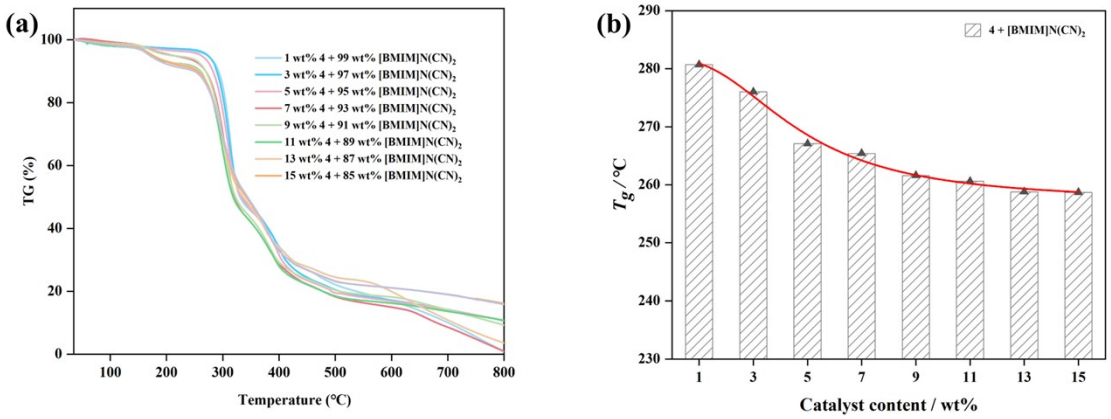

Fig. S9 Decomposition temperatures (a) and variation rule (b) of MOF **4** + $[BMIM]N(CN)_2$

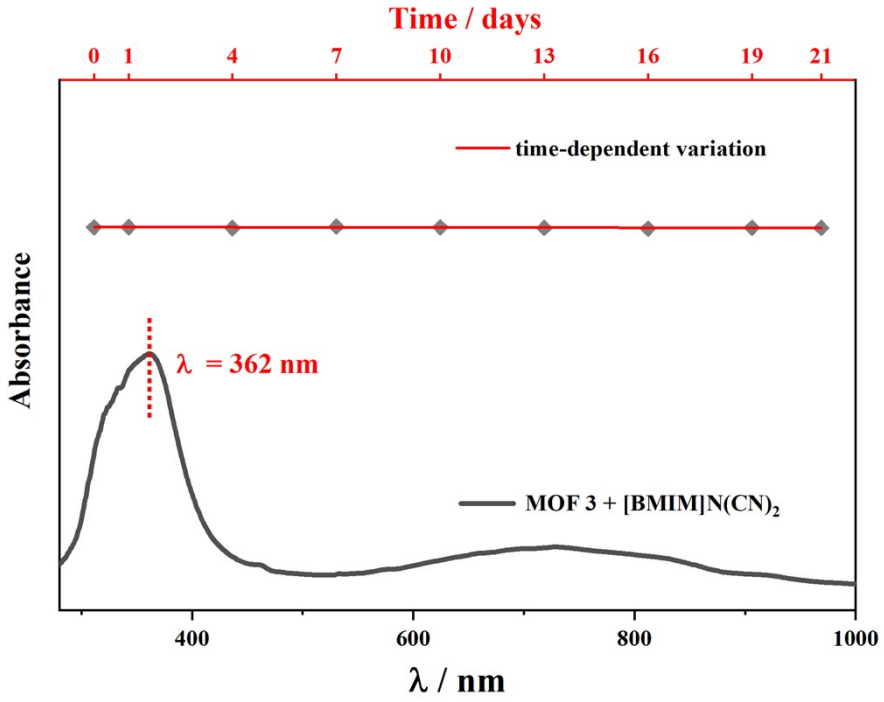

Fig. S10 UV-vis spectra of MOF **3** + $[BMIM]N(CN)_2$ and its absorbance with time at 362 nm

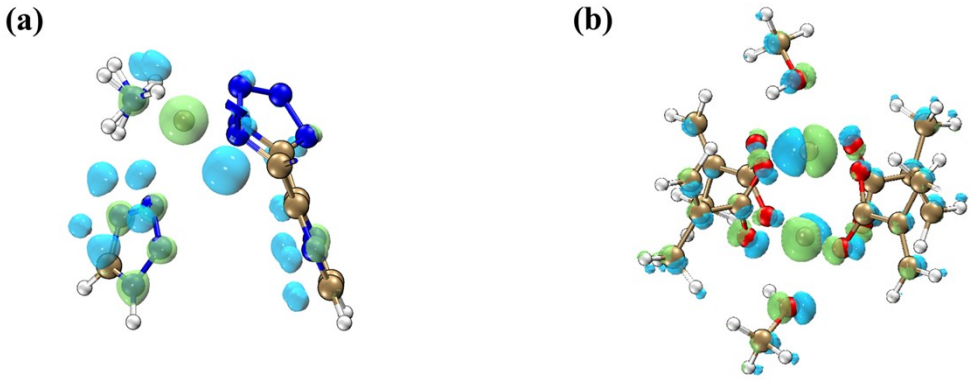

Fig. S11 The charge density difference plots for MOFs **1** (a) and **4** (b) The green and blue areas denote the electron accumulation and depletion regions, respectively. The C, N, O, Cu, and H atoms are represented by gold, blue, red, silver white balls, respectively

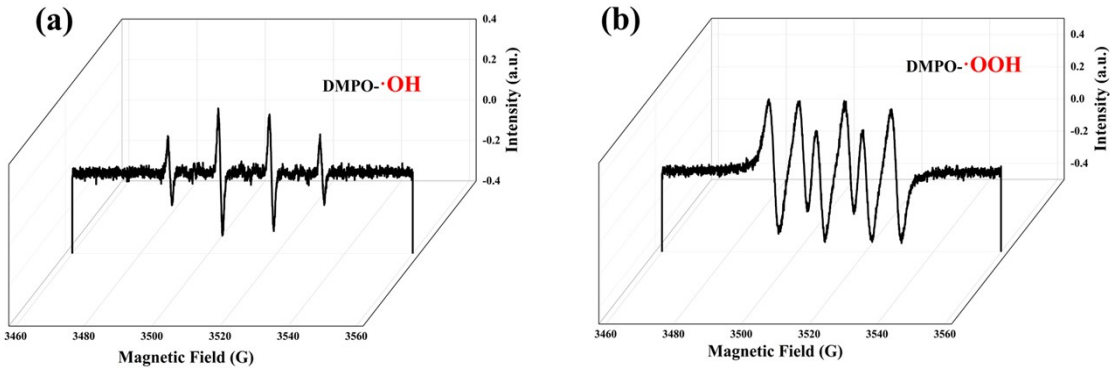

Fig. S12 EPR spectra (a) DMPO-·OH and (b) DMPO-·OOH in MOF **1** + $[BMIM]N(CN)_2$ + H_2O_2 system

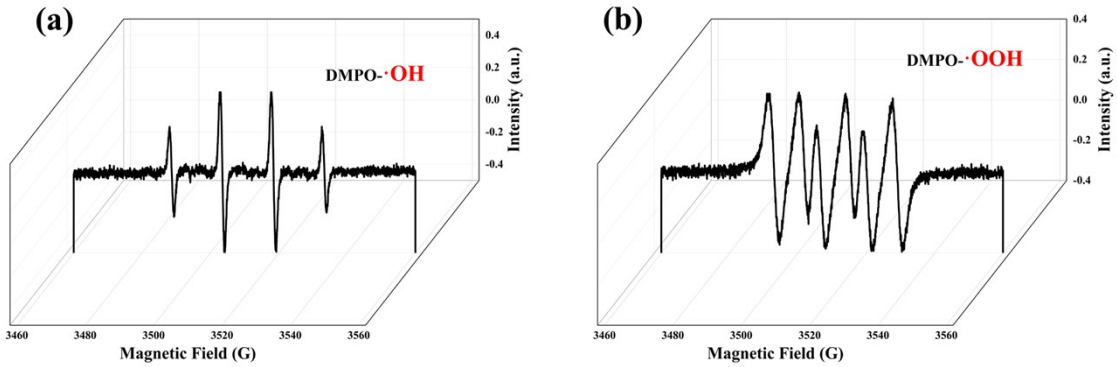

Fig. S13 EPR spectra (a) DMPO-·OH and (b) DMPO-·OOH in MOF **2** + $[BMIM]N(CN)_2$ + H_2O_2 system

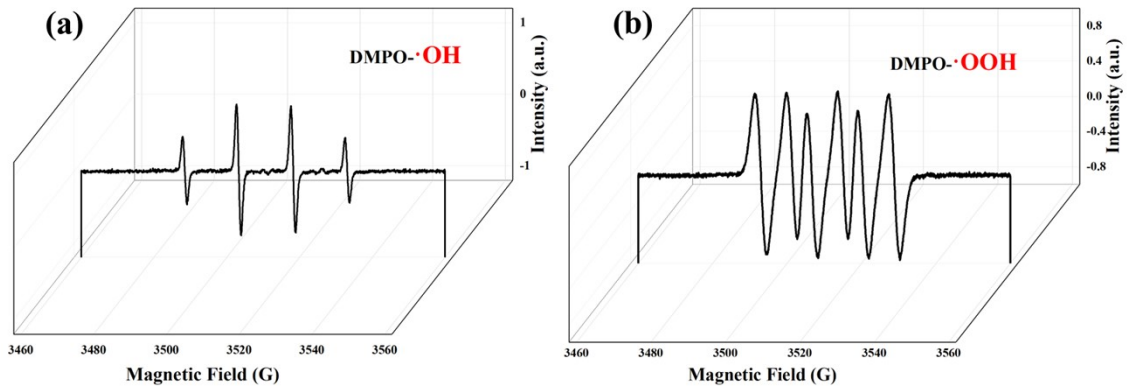

Fig. S14 EPR spectra (a) DMPO- • OH and (b) DMPO- • OOH in MOF **3** + $[BMIM]N(CN)_2$ + H_2O_2 system

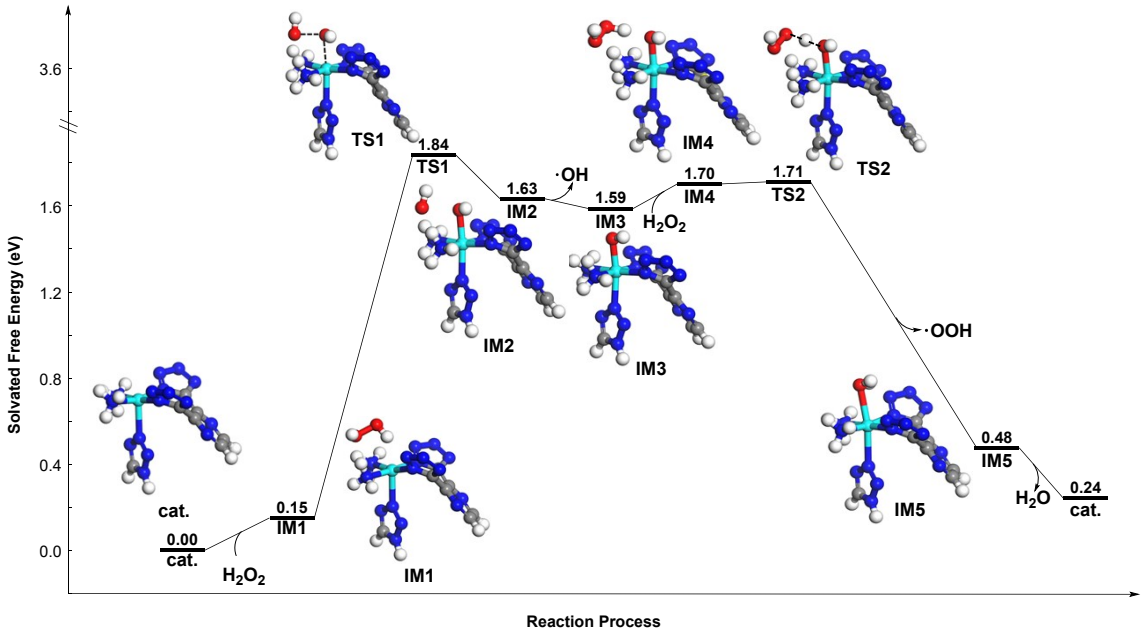

Fig. S15 DFT calculations of H_2O_2 catalysed by MOF **1**

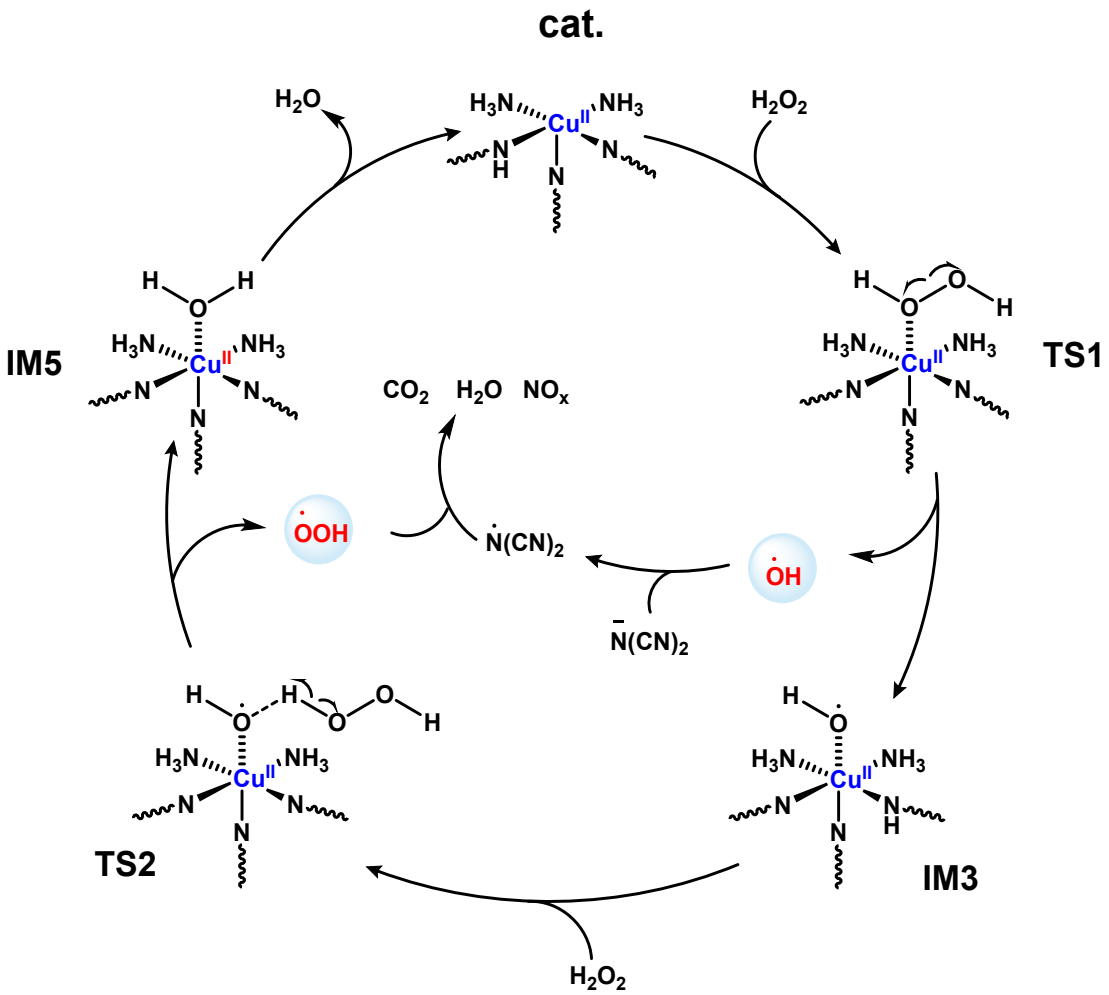

Fig. S16 Proposed catalytic mechanism of MOF **1** as catalyst